A novel geometric analysis of the kinematics of the 3-R$\underline{P}$S manipulator

Teja Krishna Mamidi[1], Aravind Baskar[2] and Sandipan Bandyopadhyay[3]

[1]*Dept. of Engineering Design, Indian Institute of Technology Madras, Chennai-600 036, India, e-mail: tejaiiit27@gmail.com*
[2]*Dept. of Engineering Design, Indian Institute of Technology Madras, Chennai-600 036, India, e-mail: krishna.arvind91@gmail.com*
[3]*Dept. of Engineering Design, Indian Institute of Technology Madras, Chennai-600 036, India, e-mail: sandipan@iitm.ac.in*

Abstract. This paper looks at the forward kinematics problem of the 3-R$\underline{P}$S manipulator from a geometric perspective. It shows that the problem is equivalent to finding the intersection of a pair of quad-circular octic curves with a circle. The results explain all the known algebraic results in this regard, and provide an intuitive insight into the nature of the solutions, as regards the operation modes, and the assembly modes inside each. The theoretical results are illustrated with a numerical example, where all the 16 assembly modes are real.

Key words: 3-R$\underline{P}$S manipulator, Forward Kinematic Univariate (FKU), Operation modes, Constraint surfaces, Quad-circular octic curve.

1 Introduction

Forward kinematic (FK) problem of the 3-R$\underline{P}$S manipulator has been studied in detail in the past [7, 2]. In a recent contribution, Schadlbauer et al. present a detailed algebraic analysis using the Study parameter representation of $\mathbb{SE}(3)$, leading to the identification of the two operation modes of the manipulator. In this paper, a novel geometric approach to the problem is proposed, in which the manipulator is decomposed into two kinematic sub-chains, namely, a spatial RSSR chain, and a planar RP chain. The FK problem reduces to the intersection of the circle generated by the second chain with the surface generated by the first one, once all the inputs are given. While this idea has been mentioned in [3], the authors were not able to find any published reports using this approach. The authors retrieve the fact that there are up to 16 possible assembly modes, counting the pair-wise mirrored modes at the base plane. Also, the two operation modes reported in [6] show up in these results, in a new and interesting manner. The geometric interpretation of the FK could lead to an intuitive understanding of the singularities of the manipulator, which is yet to be studied.

The rest of the paper is organised as follows: the geometric formulation of the FK problem, followed by a numerical example is presented in Section 2. The new

results are interpreted geometrically and corroborated with the existing results in Section 3. Finally, the conclusions are presented in Section 4.

2 Geometric formulation of the FK problem

The FK problem is formulated below, as a geometric problem of finding the intersections of a surface and a circle in $\mathbb{R}^3$.

2.1 Geometry of the 3-R<u>P</u>S manipulator

The 3-R<u>P</u>S manipulator consists of three legs, each of which is an R<u>P</u>S-serial chain connected to the fixed platform $\boldsymbol{b}_1\boldsymbol{b}_2\boldsymbol{b}_3$ by a revolute joint, and to the moving platform $\boldsymbol{p}_1\boldsymbol{p}_2\boldsymbol{p}_3$ by a spherical joint, as shown in Fig. 1a. The said platforms are equilateral triangles in shape, with circumradii b and a respectively. The manipulator has three degrees-of-freedom (DoF), which are activated by the prismatic actuators denoted by $\boldsymbol{l} = [l_1, l_2, l_3]^\top$, while the revolute joints are *passive*. These joint angles, denoted by $\boldsymbol{\phi} = [\phi_1, \phi_2, \phi_3]^\top$ form the unknowns to be obtained as a result of the FK problem. The fixed frame of reference $\{A\}$, given by $\boldsymbol{o}_A$-$\boldsymbol{X}_A\boldsymbol{Y}_A\boldsymbol{Z}_A$, is attached to the centre of the base platform, while the moving frame of reference $\{B\}$, by $\boldsymbol{o}_B$-$\boldsymbol{X}_B\boldsymbol{Y}_B\boldsymbol{Z}_B$, is attached at the centre of the moving platform. The vertices of the fixed and moving platforms are found as: ${}^A\boldsymbol{b}_1 = [b,0,0]^\top$, ${}^A\boldsymbol{b}_2 = \left[-\frac{b}{2}, \frac{\sqrt{3}b}{2}, 0\right]^\top$, ${}^A\boldsymbol{b}_3 = \left[-\frac{b}{2}, -\frac{\sqrt{3}b}{2}, 0\right]^\top$; and ${}^A\boldsymbol{p}_1 = {}^A\boldsymbol{b}_1 + [-l_1\cos\phi_1, 0, l_1\sin\phi_1]^\top$, ${}^A\boldsymbol{p}_2 = {}^A\boldsymbol{b}_2 + \left[\frac{l_2}{2}\cos\phi_2, -\frac{\sqrt{3}l_2}{2}\cos\phi_2, l_2\sin\phi_2\right]^\top$, ${}^A\boldsymbol{p}_3 = {}^A\boldsymbol{b}_3 + \left[\frac{l_3}{2}\cos\phi_3, \frac{\sqrt{3}l_3}{2}\cos\phi_3, l_3\sin\phi_3\right]^\top$, respectively.

The objective of the FK problem is to determine the position and orientation of the moving platform. This can be achieved if the unknown passive angles, ϕ_i, can be obtained from the knowledge of the inputs l_j. Three *independent* equations need to be formed, relating ϕ_i to l_j, which is accomplished below using the concept of kinematic sub-chains.

2.2 Derivation of the constraints

The manipulator is hypothetically decomposed into two sub-chains, by removing the spherical joint at point $\boldsymbol{p}_1$, as shown in Fig. 1. This leads to two hypothetically distinct points: $\boldsymbol{p}_{s_1}$, which is a *coupler point* of the spatial RSSR mechanism $\boldsymbol{b}_2\boldsymbol{p}_2\boldsymbol{p}_3\boldsymbol{b}_3$; and $\boldsymbol{p}_{c_1}$, which is the tip of the serial chain $\boldsymbol{b}_1\boldsymbol{p}_1$. Obviously, the points $\boldsymbol{p}_{s_1}$ and $\boldsymbol{p}_{c_1}$ *must* coincide to form the original point $\boldsymbol{p}_1$ in the manipulator. Equivalently, the

(a) 3-R$\underline{P}$S manipulator
(b) sub-chains
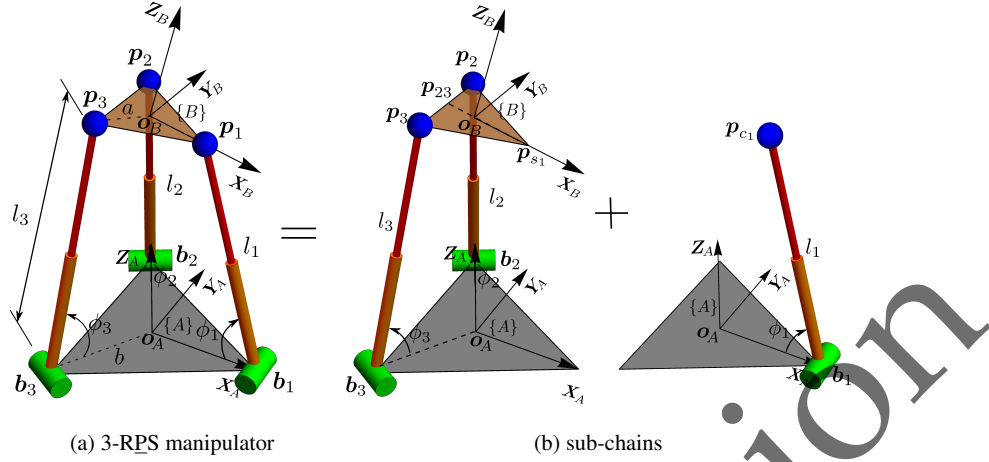
Fig. 1: 3-R$\underline{P}$S manipulator decomposition into sub-chains

locus of $\boldsymbol{p}_{s_1}$, which is a surface, must intersect the locus of $\boldsymbol{p}_{c_1}$, i.e., a circle in the plane $\boldsymbol{o}_A \boldsymbol{b}_1 \boldsymbol{p}_1$ (see Fig. 1).

2.2.1 Derivation of the coupler surface, $S = 0$

Let $^A\boldsymbol{p}_{s_1} = {}^A\boldsymbol{p}_{c_1} = {}^A\boldsymbol{p}_1 = [x,y,z]^\top$. Once the inputs l_2, l_3 are frozen, the locus of $\boldsymbol{p}_{s_1}$, which can be interpreted as the *coupler surface* of the said RSSR chain, is described in terms of five unknown variables, namely, ϕ_2, ϕ_3, x, y, z. These variables need to satisfy the following constraints:

- The first constraint is derived from the closure of the RSSR loop. This is equivalent of noting that the distance between $^A\boldsymbol{p}_2$ and $^A\boldsymbol{p}_3$ is equal to $\sqrt{3}a$:

$$g_1(\phi_2, \phi_3, x, y, z) \triangleq ({}^A\boldsymbol{p}_3 - {}^A\boldsymbol{p}_2) \cdot ({}^A\boldsymbol{p}_3 - {}^A\boldsymbol{p}_2) - 3a^2 = 0. \tag{1}$$

- The other two constraints are derived from the fact that the locus of $\boldsymbol{p}_{s_1}$, *with respect to the points $\boldsymbol{p}_2 \boldsymbol{p}_3$,* is a circle, in a plane that bisects $\boldsymbol{p}_2 \boldsymbol{p}_3$ perpendicularly. In effect, this defines a *virtual rigid link $\boldsymbol{p}_{23} \boldsymbol{p}_{s_1}$*, which has a rotary joint at $\boldsymbol{p}_{23}$, with an axis aligned with $\boldsymbol{p}_2 \boldsymbol{p}_3$. Orthogonality of the virtual link to $\boldsymbol{p}_2 \boldsymbol{p}_3$ is captured by the constraint:

$$g_2(\phi_2, \phi_3, x, y, z) \triangleq ({}^A\boldsymbol{p}_{23} - {}^A\boldsymbol{p}_{s_1}) \cdot ({}^A\boldsymbol{p}_3 - {}^A\boldsymbol{p}_2) = 0. \tag{2}$$

Rigidity of the virtual link leads to the third and final constraint:

$$g_3(\phi_2, \phi_3, x, y, z) \triangleq ({}^A\boldsymbol{p}_{23} - {}^A\boldsymbol{p}_{s_1}) \cdot ({}^A\boldsymbol{p}_{23} - {}^A\boldsymbol{p}_{s_1}) - \frac{9a^2}{4} = 0. \tag{3}$$

The unknown ϕ_2 is easily eliminated from Eqs. (1, 3), which are linear in $\sin\phi_2$ and $\cos\phi_2$. This leads to the eliminant $h_1(\phi_3, x, y, z) = 0$, while substitution of $\sin\phi_2$ and $\cos\phi_2$ into Eq. (2) leads to $h_2(\phi_3, x, y, z) = 0$. The function h_1 is of degree four in $\cos\phi_3$, $\sin\phi_3$, while h_2 is linear in these. Converting $h_i = 0$ to their algebraic forms in $t_3 = \tan(\phi_3/2)$ one obtains the equations $s_i(t_3, x, y, z) = 0$, $i = 1, 2$. The equation of the coupler surface, $S(x, y, z) = 0$, which is of degree 20 in x, y, z and even powered in z, is obtained by eliminating t_3 between the last two equations. The process of elimination is depicted in schematic (4) below:

$$
\left.
\begin{array}{l}
h_1(\phi_3, x, y, z) = 0 \xrightarrow{\phi_3 \to t_3} s_1(t_3, x, y, z) = 0 \\
h_2(\phi_3, x, y, z) = 0 \xrightarrow{\phi_3 \to t_3} s_2(t_3, x, y, z) = 0
\end{array}
\right) \xrightarrow{\times t_3} S(x, y, z) = 0. \tag{4}
$$

The symbol '$\xrightarrow{\phi_3 \to t_3}$' denotes the conversion of the equations preceding it, into their algebraic form in $t_3 = \tan(\phi_3/2)$. The symbol '$\xrightarrow{\times t_3}$' represents the elimination of the variable t_3 from the equations preceding it.

2.2.2 Derivation of the circular constraint, $C = 0$

The point $\boldsymbol{p}_{c_1}$ describes a circle in the plane $\boldsymbol{o}_A \boldsymbol{b}_1 \boldsymbol{p}_1$, by virtue of the rotary joint at $\boldsymbol{b}_1$. This can be captured in terms of algebraic equations as follows.

- Rigidity of leg 1 (given the input l_1), expressed in terms of the leg-length constraint, describes a *sphere* of radius l_1, centered at $\boldsymbol{b}_1$:

$$
\zeta_1(x, y, z) \triangleq ({}^A\boldsymbol{p}_{c_1} - {}^A\boldsymbol{b}_1) \cdot ({}^A\boldsymbol{p}_{c_1} - {}^A\boldsymbol{b}_1) - l_1^2 = 0. \tag{5}
$$

- Axis of the rotary joint at $\boldsymbol{b}_1$ is along $\boldsymbol{e}_{Y_A} = [0, 1, 0]^\top$, which leads to the *planarity constraint*:

$$
\zeta_2(y) \triangleq ({}^A\boldsymbol{p}_{c_1} - {}^A\boldsymbol{b}_1) \cdot \boldsymbol{e}_{Y_A} = 0 \tag{6}
$$

$$
\Rightarrow y = 0. \tag{7}
$$

The locus of the point $\boldsymbol{p}_{c_1}$ is established as a circle of radius l_1 centered at $\boldsymbol{b}_1$, by cutting the sphere in Eq. (5) by the plane $y = 0$. The equation of the circle, denoted as $C(x, z) = 0$, is obtained by substituting $y = 0$ in Eq. (5).

2.3 Derivation of the Forward Kinematic Univariate (FKU)

The FK problem may be solved by computing the intersections of the surface $S = 0$ with the circle $C = 0$. However, the same may also be reduced by first cutting the surface $S = 0$ by the plane $y = 0$ to obtain the curve $C' = 0$ in the $\boldsymbol{X}_A \boldsymbol{Z}_A$ plane,

and then obtaining the intersections of $C' = 0$ with $C = 0$. An advantage of this approach is that the curve $C' = 0$ decomposes into three components (see Fig. 2 for an illustration, and Section 3 for a detailed interpretation of the same), as shown in schematic 8:

$$S(x,y,z) = 0 \xrightarrow{y \to 0} C'(x,z) = C'_0(x,z)C'_1(x,z)C'_2(x,z) = 0. \tag{8}$$

The component $C'_0(x,z) = (x+2b)^2 + z^2 = 0$ admits a real solution *iff* $x = -2b$ and $z = 0$. For these values of x, z the constraint equations given by Eqs. $(1,2,3,5)$ in Sections 2.2.1, 2.2.2 are consistent *iff* the input parameters satisfy the following conditions:

$$l_2^2 = l_3^2 = 3a^2 - 3b^2, \; l_1^2 = 9b^2. \tag{9}$$

The conditions in Eq. (9) correspond to the finite self-motion of the manipulator reported in [5]. Hence, the factor C'_0 is ignored in the following analysis. The implications of the said factor in relevance to the sub-chains have been discussed in [1]. The components $C'_i, i = 1, 2$ are of degree 8 in x, z and they describe the two *operation modes* of the manipulator. Bézout limit puts the possible number of intersections with a circle at 16. However, the components of C'_i describe very special octic curves—these are quad-circular in nature. Therefore, 4 pairs of points of intersection lie in the plane at infinity, thus limiting the number of finite complex solutions to only 8, per mode.

Vanishing of the resultant of $C'_1(x,z)$ with $C(x,z)$ w.r.t. x leads to the desired FKU equation, namely, $\xi_1(z) = 0$, for the mode 1.

$$\left. \begin{array}{l} C'_1(x,z) = 0 \\ C(x,z) = 0 \end{array} \right) \xrightarrow{\times x} \xi_1(z) = 0 \; , \; \left. \begin{array}{l} C'_2(x,z) = 0 \\ C(x,z) = 0 \end{array} \right) \xrightarrow{\times x} \xi_2(z) = 0.$$

A similar computation leads to $\xi_2(z) = 0$, the FKU equation for the second mode. These equations have been derived in closed-form, whereupon it is observed that the FKUs are both of degree four in z^2, and they maintain the relationship:

$$\xi_1(a) = \xi_2(-a), \tag{10}$$

where a is the circumradius of the moving platform.

2.4 Numerical example

The formulation presented above is illustrated for the following set of numerical values: $a = 1/2$, $b = 1$, $l_1 = 11/5$, $l_2 = 23/10$ and $l_3 = 12/5$. The length dimensions are scaled by the radius of the circum-circle of the base triangle, b, rendering them unit-less, while all angles are measured in radians. It may be noted that the rational values of the numeric parameters help in retaining the *exact* nature of the

Table 1: Sixteen real solutions to forward kinematics problem

Operation mode	Assembly mode	z	x	ϕ_1	ϕ_2	ϕ_3	x_0	x_1
Mode 1	1	2.197	0.889	1.520	0.899	0.860	0	-0.268
	2	-2.197	0.889	-1.520	-0.899	-0.860	0	-0.268
	3	1.721	-0.371	0.898	1.465	0.831	0	-0.393
	4	-1.721	-0.371	-0.898	-1.465	-0.831	0	-0.393
	5	1.660	-0.443	0.855	0.829	1.386	0	-0.540
	6	-1.660	-0.443	-0.855	-0.829	-1.386	0	-0.540
	7	1.627	-0.480	0.833	0.853	0.912	0	-0.987
	8	-1.627	-0.480	-0.833	-0.853	-0.912	0	-0.987
Mode 2	1	2.178	0.687	1.428	0.781	1.264	-0.469	0
	2	-2.178	0.687	-1.428	-0.781	-1.264	-0.469	0
	3	2.165	0.609	1.392	1.298	0.754	-0.400	0
	4	-2.165	0.609	-1.392	-1.298	-0.754	-0.400	0
	5	2.139	0.485	1.335	1.355	1.355	-0.993	0
	6	-2.139	0.485	-1.335	-1.355	-1.355	-0.993	0
	7	1.597	-0.513	0.812	1.390	1.320	-0.565	0
	8	-1.597	-0.513	-0.812	-1.390	-1.320	-0.565	0
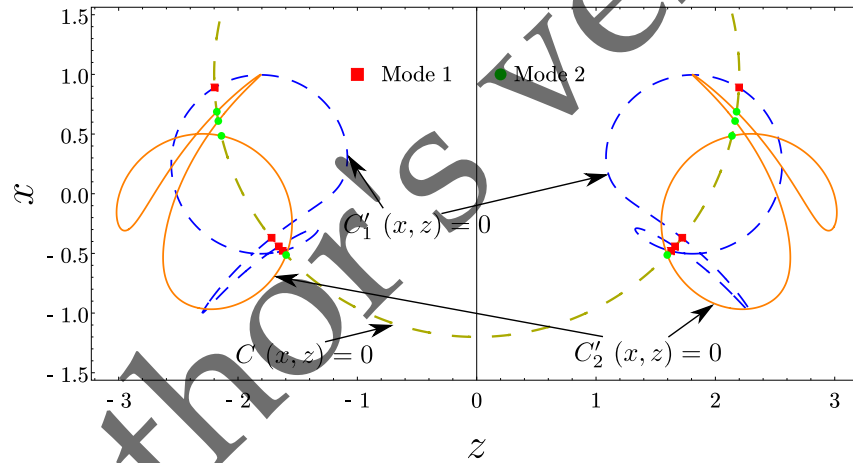
Fig. 2: Constraint geometries in the plane $\boldsymbol{X}_A\boldsymbol{Z}_A$: $C_i' = 0$ and $C = 0$

computation up to the values of the coefficients of the FKU equations. The monic forms of these, for the given values, are[1]:

---

[1] Though the coefficients are obtained as exact rational numbers, their real approximations are presented here for the want of space.

$$\xi_1 = u^4 - 13.193u^3 + 63.689u^2 - 134.113u + 104.347,$$

$$\xi_2 = u^4 - 16.554u^3 + 101.072u^2 - 268.351u + 259.275, \text{ where } u = z^2.$$

Each operation mode contains 8 real assembly modes for these numbers. The results have been tabulated in Table. 1. The solutions are visualised as the points of intersection of the constraint curves $C_i' = 0$ and $C = 0$, as seen in Fig. 2.

3 Interpretation of the results and correlation with existing ones

The algebraic properties of the FKU of the 3-RPS manipulator have been studied and reported at length. Yet, there has been no attempt to bring out the coherence between these results, and to visualise them geometrically. For instance, [6] reports the two operational modes, each characterised by the vanishing of one of the two Stüdy parameters, x_1 and x_0. In physical terms, this means that in the latter case, the moving platform rotates through π about a horizontal axis. In [4] the FKU is derived from the constraint equations in the joint-space, and it is found that the FKU factors in two components, g_1 and g_2, where $g_1(a) = g_2(-a)$, a being the circum-radius of the moving platform. It may be noted that this is *consistent* with the findings in [6], since a going to $-a$ is identical in effect with the *flipping* of the moving platform *up-side down*, which is same as the π-*screw* motion described in [6]—in either case, a CCW distribution of the vertices $\boldsymbol{p}_1$, $\boldsymbol{p}_2$, $\boldsymbol{p}_3$ changes into a CW one.

The results of the present work corroborate and unify all of the results on FK reported in [6, 4]. The relationship with the results in [4] is captured by Eq. (10), where ξ_i play the roles of g_i in [4]. Also, the FKU is found to have only the even powers in either mode, signifying the manipulator poses are reflected pairwise at the base platform. On the other hand, as seen in Table 1, the vanishing of x_0 and x_1 in one of the two modes confirm the corroboration with the results of [6].

Figure 2 presents a visual summary of the algebraic results, which can be considered as a new contribution of the present work. The curve $C'(x,z) = 0$ decomposes into its components $C_1'(x,z) = 0$ and $C_2'(x,z) = 0$, signifying the two modes. Also, the reflections of each mode at the $z = 0$ line are obvious in the figure. Thus, these pictures provide a complete understanding of all the operations modes, and the assembly modes therein. These interpretations can be extended easily into the domain of singularity analysis and design.

4 Conclusion

This paper presents a geometric analysis of the 3-RPS manipulator. The manipulator is decomposed into two kinematic sub-chains, and the forward kinematic problem is formulated as the geometric problem of finding the intersections of the constraint varieties generated by the individual sub-chains. A new result is revealed in the

process, that the problem is equivalent to the intersection of a circle with a pair of quad-circular octic curves in the plane of the circle. All the existing algebraic results reported in [4, 6, 7] are explained from the same geometric perspective. The results show striking similarities with those known in the case of the planar 3-RRR manipulator, whose forward kinematic problem is equivalent to the intersection of a tri-circular sextic curve with a circle. On the other hand, other spatial manipulators, such as the 3-RRS, which have architectural similarities with the 3-RPS, may be analysed in the same geometric framework, leading, hopefully, to analogous results. Also, these geometric interpretations may lead to a better understanding of the singularities of these manipulators, which is to be studied next.

References

1. Bandyopadyay, S., Mamidi, T.K., Baskar, A.: Kinematic analysis of the 3-RPS manipulator using the geometry of plane curves (2017). Submitted for presentation in Proceedings of the International Symposium of Mechanism and Machine Science, Azerbaijan Technical University, Baku, Azerbaijan.
2. Ghosal, A.: Robotics: Fundamental Concepts and Analysis. Oxford University Press, New Delhi (2006)
3. Gosselin, C.: Kinematic analysis, optimization and programming of parallel robotic manipulators. Ph.D. thesis, Department of Mechanical Engineering, McGill University, Montreal, Canada (1988)
4. Rangaprasad, A.S., Bandyopadhyay, S.: Analysis of constraint equations and their singularities. In: J. Lenarcic, O. Khatib (eds.) Advances in Robot Kinematics, pp. 429–436. Springer International Publishing, Switzerland (2014)
5. Schadlbauer, J., Husty, M.L., Caro, S., Wenger, P.: Self-motions of 3-RPS manipulators. Frontiers of Mechanical Engineering **8**(1), 62–69 (2013)
6. Schadlbauer, J., Walter, D.R., Husty, M.L.: The 3-RPS parallel manipulator from an algebraic viewpoint. Mechanism and Machine Theory **75**, 161–176 (2014)
7. Tsai, L.W.: Robot Analysis: The Mechanics of Serial and Parallel Manipulators. John Wiley & Sons Inc., New York (1999)

5 Acknowledgment